Emulsification failure in a ternary microemulsion

M. Leaver, U. Olsson, H. Wennerström, R. Strey

▶ **To cite this version:**

M. Leaver, U. Olsson, H. Wennerström, R. Strey. Emulsification failure in a ternary microemulsion. Journal de Physique II, 1994, 4 (3), pp.515-531. 10.1051/jp2:1994142 . jpa-00247976

HAL Id: jpa-00247976
https://hal.science/jpa-00247976

Submitted on 4 Feb 2008

HAL is a multi-disciplinary open access archive for the deposit and dissemination of scientific research documents, whether they are published or not. The documents may come from teaching and research institutions in France or abroad, or from public or private research centers.

L'archive ouverte pluridisciplinaire **HAL**, est destinée au dépôt et à la diffusion de documents scientifiques de niveau recherche, publiés ou non, émanant des établissements d'enseignement et de recherche français ou étrangers, des laboratoires publics ou privés.

Classification
Physics Abstracts
82.70D — 61.20Q — 76.60E

Emulsification failure in a ternary microemulsion

M. S. Leaver ([1]), U. Olsson ([1]), H. Wennerström ([1]) and R. Strey ([2])

([1]) Physical Chemistry 1, University of Lund, Chemical Center, P.O. Box 124, S-221 00 Lund, Sweden
([2]) Max-Planck-Institut für Biophysikalische Chemie, Postfach 2841, D-37018 Göttingen, Germany

(*Received 21 June 1993, revised 16 November 1993, accepted 23 November 1993*)

Abstract. — The microstructure of the water rich microemulsion phase of the $C_{12}E_5$, water and decane system has been studied using surfactant ^{2}H-NMR relaxation and ^{1}H Fourier transform pulsed gradient spin-echo (FTPGSE) self-diffusion experiments. The surfactant-to-oil ratio is kept constant, and the system is investigated as a function of water dilution and temperature. Particular attention is focused at the phase boundary where the microemulsion, consisting of normal oil swollen micelles is in equilibrium with excess oil. On this phase boundary, which occurs at lower temperatures, the oil-swollen micelles adopt a minimum size, and it is argued that this corresponds to a spherical shape. Increasing the temperature, the micelles grow in size. However, the results indicate that the micellar growth is only minor, in particular at lower concentrations. The implications of the experimental results and the phase equilibria are discussed within the frame work of the flexible surface model, associating a curvature energy to the surfactant film. The behaviour of the system is consistent with a monotonic variation of the spontaneous mean curvature of the surfactant monolayer with temperature. The phase equilibrium with excess oil can be identified with a so-called emulsification failure. Over a large dilution range, $\Phi \leq 0.35$, the emulsification failure boundary occurs at constant temperature and surfactant-to-oil ratio, which, within the model, imposes a lower limit to the possible values of the monolayer bending rigidity.

1. Introduction.

Oil and water are normally immiscible but the addition of a suitable amphiphilic surfactant, preferably insoluble in both oil and water, can promote stable mixtures, with the surfactant residing at the oil/water interface. With certain mixtures of the three components it is possible to form a low viscosity transparent liquid phase, known as a microemulsion. Whilst these systems are homogeneous on a macroscopic length scale they exhibit structure on a microscopic scale (10-1 000 Å), where the apolar and polar domains are separated by the surfactant rich film. The size, number or curvature of these interfaces are not fixed, rather they are determined by the system's equilibrium conditions which minimize the free energy of the film. Dependent on the concentration of the components and temperature of the mixture, the

curvature of the surfactant film may alter to enclose a finite volume of oil or water, in the form of normal or reversed micelles respectively, or form a three-dimensional continuous dividing surface of multiply connected topology in a bicontinuous microstructure.

In order to study the properties of microemulsion systems theoretically it is possible to treat the surfactant monolayer as a flexible, elastic but incompressible surface. Using the curvature energy concept [1] the surfactant film is treated as geometric surface with each configuration of the surface assigned a curvature free energy, G_c. The curvature free energy of a given surface configuration is then calculated as the surface (Σ) integration of the local curvature free energy density, g_c, and hence

$$G_c = \int_{\Sigma} dA g_c \,. \tag{1}$$

The total free energy of the system is now obtained by a summation over all the allowed configurations of the surface using a Boltzmann weighting factor.

The local curvature free energy density is usually expanded to the second order in the curvatures. In this case g_c is expressed in the form [1, 2]

$$g_c = \kappa (H - H_0)^2 + \bar{\kappa} K \tag{2}$$

where H is the mean curvature, H_0 the spontaneous mean curvature, and K is the Gaussian curvature. The two expansion coefficients are the bending rigidity (κ) and the saddle splay coefficient ($\bar{\kappa}$). The saddle splay constant takes into account the energy cost to the system in allowing the amphiphilic interface to adopt saddle like deformations and the bending rigidity allows for the resistance, or lack of it, to the interface adopting conformations away from that dictated by the natural radius of curvature.

Balanced microemulsions and related systems, such as L_3 phases, occur mainly in the absence of long-range interactions, i.e. with effectively uncharged surfactant films. For such systems [3-7] it is advantageous, experimentally, to use non-ionic surfactants (for example of the ethylene oxide type) since the various systems can be prepared with the minimum number of components. Furthermore, phase diagrams and structural transitions observed when increasing the temperature show that with this type of surfactant the spontaneous curvature of the surfactant film decreases monotonically with increasing temperature [8, 9]. For example, considering sections at constant surfactant concentration through the phase prism [5-9], one observes that at lower temperatures a water-rich microemulsion and an oil-rich L_3 phases are stable. Here, the average mean curvature of the surfactant monolayer is towards the oil, $\langle H \rangle > 0$. At higher temperatures an oil-rich microemulsion and a water rich L_3 phase is stable. Here, $\langle H \rangle < 0$. At an intermediate temperature, a « balanced » microemulsion (a bicontinuous microemulsion containing equal amounts of water and oil) is stable and a marked stability of a lamellar phase is observed with $\langle H \rangle = 0$. This behaviour can be understood within the flexible surface model by assuming that the spontaneous mean curvature, H_0, of the surfactant monolayer decreases with increasing temperature as discussed above [8]. This notion has formed the basis for our understanding of microemulsions and L_3 phases with non-ionic surfactant [8, 10].

The present communication deals with a water rich microemulsion composed of pentaethylene glycol dodecyl ether ($C_{12}E_5$), water and decane. The surfactant-to-oil volume fraction ratio, Φ_s/Φ_0, has been kept constant, at a value of 0.815, so that we are studying an area in the concentration-temperature phase prism as illustrated in figure 1a. The phase diagram [11] for the temperature dependence as a function of Φ, the particle volume fraction ($\Phi \equiv \Phi_s + \Phi_0$), is shown in figure 1b. We emphasize here that keeping Φ_s/Φ_0 constant corresponds to fixing

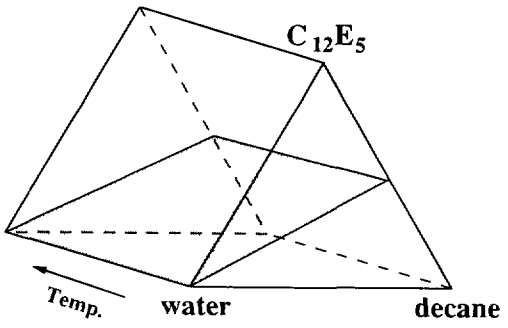

a)

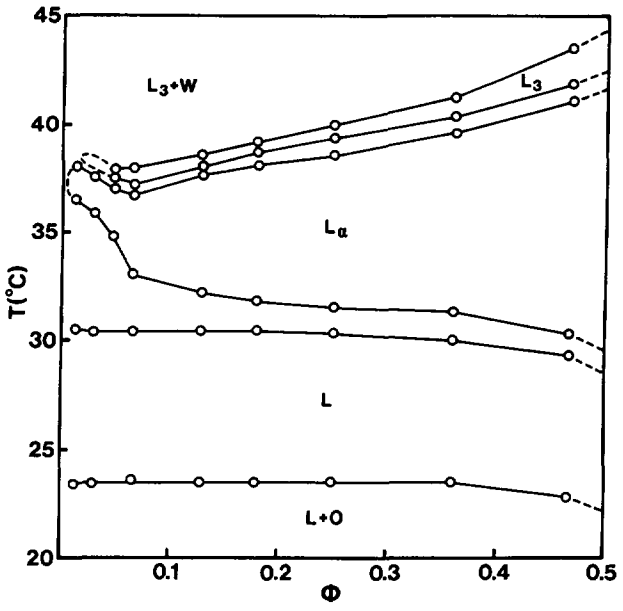

b)

Fig. 1. — a) An illustration of the section through the phase prism, defined by a constant surfactant-to-oil ratio, $\Phi_s/\Phi_0 = 0.815$. b) A partial phase diagram, reproduced from reference [11], of the system $C_{12}E_5/^2H_2O$/decane, at a constant surfactant-to-oil ratio $\Phi_s/\Phi_0 = 0.815$. The phase diagram is drawn as temperature *versus* Φ, where Φ denotes the volume fraction of surfactant + oil. L is a liquid microemulsion phase, L_α denotes a lamellar liquid crystalline phase and L_3 is a bilayer continuous liquid phase.

the total area to enclosed volume ratio, since the area per surfactant molecule is independent of the aggregate geometry and temperature [12].

In this system a microemulsion phase, L, is stable within a limited temperature range. Increasing the temperature, first a lamellar phase, L_α, is formed which, with a further increase in temperature, transforms to a liquid L_3 or « sponge phase », which at higher temperatures is in equilibrium with almost pure water. In the microemulsion phase the mean curvature of the surfactant film is on the average towards oil, in the lamellar phase it is zero while in the L_3

phase it is towards water. The phase diagram is very similar to the phase diagram of the binary water $C_{12}E_5$ system [13]. The major exception is that in the presence of oil the stability of the L-phase is limited at lower temperatures. At temperatures below the lower phase boundary the microemulsion is in equilibrium with almost pure oil. It is remarkable that the lower phase boundary is temperature insensitive over a wide concentration range.

The phase sequence observed when varying the temperature (Fig. 1b), is consistent with a decreasing spontaneous mean curvature with increasing temperature, where this value even change sign in the vicinity of the lamellar phase. To investigate this relation further, and to further compare system with the predictions of the flexible surface model it is of interest to study the structural variation with temperature within the microemulsion phase. In particular along the lower phase boundary, below which there is an incomplete solubilization of the oil.

Safran *et al.* [14, 15] have studied the relative stability of different geometrical shapes, such as spheres, cylinders and lamellae, as a function of H_0 and the elastic constants. Considering normal, oil-swollen micelles transitions from spheres to cylinders to lamellae are predicted as a function of decreasing H_0 (here and in what follows, we adopt the convention that curvature towards oil is counted as positive). Furthermore, for a given surfactant-to-oil ratio, corresponding to a given total interfacial area-to-enclosed volume, there is an upper limit of H_0 above which the microemulsion expels a separate oil phase, since the curvature energy favours smaller droplets having a higher surfactant-to-oil ratio. This latter phenomenon has been termed the emulsification failure (EF) [14]. Hence, the predictions from curvature energy considerations are that spherical micelles should be stable in the vicinity of the lower phase boundary and that the micelles should grow into a cylindrical shape with increasing temperature.

A suitable experimental technique for investigating variations in micellar size is ^{2}H-NMR relaxation time measurements, using a selectively deuterated surfactant. The advantages of this technique is the strong dependence of the transverse relaxation rate on the micellar size and, since it monitors reorientational dynamics, there is a negligible influence of intermicellar interactions (except for the case of overlapping cylindrical micelles and similar cases when the rotational diffusion of the aggregate is sterically hindered). The latter advantage is particularly important to consider, since for the observables of most other techniques, such as for example, static light scattering intensity, collective and self-diffusion coefficients, viscosity etc., the interplay of micellar size and interaction effects are often difficult to separate. In this respect, NMR-relaxation is comparable to form factor determinations using small angle scattering.

Focusing on the L-phase and in particular on its lower phase boundary, we have performed a ^{2}H-NMR relaxation study using selectively deuterated $C_{12}E_5$. In addition to the relaxation experiments, we have also monitored the temperature dependence of the oil and surfactant self-diffusion coefficients at two selected compositions. The results of the self-diffusion experiments not only support the conclusions drawn from the relaxation experiments, but also allow us to study the particle to bicontinuous topology transition. Furthermore, we have measured the collective diffusion coefficient in some dilute samples close to the lower phase boundary using dynamic light scattering.

2. Materials and methods.

The α-deuterated non ionic surfactant, $CH_3(CH_2)_{10}CD_2(OCH_2CH_2)_5OH(C_{12}E_5)$ was synthesized by Synthelec (Lund, Sweden) and was used without further purification. The decane (99.9 %) and deuterium depleted water were purchased from Sigma and also used without further treatment. The deuterium depleted water was used in the sample preparation to avoid « swamping » the signal from the surfactant for very dilute microemulsions. The

concentration of ^2H in the depleted water was reduced by a factor of 100 from that of millipore water.

The NMR samples were prepared by weighing the components into a 10 mm NMR tube and then immediately flame sealing. These samples were then homogenised by heating them in a temperature controlled water bath into the lamellar phase and gently agitating the tube regularly. When mixed, the samples were cooled and kept in the microemulsion phase until required for experiments. The phase diagram in figure 1b, which was characterized for samples made using ^2H_2O [11], could be reproduced using the above samples allowing for the expected ~ 2 °C increase in the transition temperatures upon substitution of water for ^2H_2O [16]. Here the samples were heated in the water bath and the phase transitions monitored between cross Polaroid sheets, to detect any optical birefringence of the phases.

The measurement of the longitudinal (R_1) and transverse (R_2) relaxation rates were performed on a Brucker MSL 100 NMR spectrometer operating at 15.67 MHz in a 2.35 T magnetic field. R_1 was measured by inversion recovery using composite pulses. R_2 was determined from the width of the ^2H signal at half height after a Lorentzian fit to the frequency spectrum, with a small ($< 2\ \%$) correction for magnetic field inhomogeneity. The inhomogeneity of the magnetic field was determined from comparing line width with the longitudinal relaxation rate of ^2H_2O in a separate heavy water sample. For one microemulsion sample we also measured R_2 from a spin-echo experiment. The inhomogeneity obtained from comparing this R_2 value with the corresponding line width was very similar to that obtained from the heavy water sample.

Quadrupolar splittings in the lamellar phase were recorded using the quadrupolar-echo sequence [17, 18]. The temperature of the sample was maintained, using an airflow system, to an accuracy of ± 0.1 °C.

Self-diffusion experiments at varying temperature were carried out on two of the samples previously used in the relaxation studies. The samples were transferred from the 10 mm tube into 5 mm tubes and then flame sealed and the experiments performed on a Joel FX-60 NMR spectrometer operating at 60 MHz, with an external ^2H lock and the temperature of the samples maintained to an accuracy of ± 0.3 °C as determined by a calibrated copper/constantan thermocouple. The self-diffusion coefficients were obtained using the Fourier transform pulsed gradient spin echo (FTPGSE) technique [19].

The self-diffusion diffusion constant (D) measurements were made according to Stilbs, where the length of the gradient pulse (δ) was varied at a constant gradient pulse interval (Δ) of 0.140 ms. The decay of the echo amplitude is given by the following relationship

$$A = A_0 \exp\left(-G^2 \gamma^2 D \delta^2 \left(\Delta - \frac{\delta}{3}\right)\right) \tag{3}$$

where G is the gradient field strength, γ is the gyromagnetic ratio and A_0 is the peak amplitude of the signal in the absence of the gradient pulse. The decay of the amplitude (A) as a function of δ was fit with a non-linear fit routine to calculate the self-diffusion constant of the species in question. The data were in all cases found to follow the relation above. Due to a fast exchange between different diffusion sites the effective D-value is an average. The gradient field strength was calibrated against the known self-diffusion coefficients of water [20] and tetradecane (n-$C_{14}H_{30}$) [21].

Dynamic light scattering experiments were performed at 25.0 ± 0.1 °C at a scattering angle of 90° using an AMTEC goniometer. The intensity auto correlation function was analysed with a Brookhaven correlator BI 8000.

3. NMR relaxation theory.

For a ^2H nucleus the quadrupolar mechanism determines the longitudinal (R_1) and the transverse (R_2) relaxation rates which are given by [22]

$$R_1 = \frac{3\pi^2}{40}\chi^2(2j(\omega) + 8j(2\omega)) \tag{4}$$

$$R_2 = \frac{3\pi^2}{40}\chi^2(3j(0) + 5j(\omega) + 2j(2\omega)) \tag{5}$$

where χ is the quadrupolar coupling constant and $j(\omega)$ is the reduced spectral density evaluated at the Larmor frequency (ω) of the deuteron. The dynamics of aggregated surfactant molecules have been shown to obey a time scale separation of fast local motions leaving a residual anisotropy which is averaged by a slow isotropic motion associated with the aggregate [23-27]. In this case the reduced spectral density is given by

$$j(\omega) = (1 - S^2)j_f(\omega) + S^2 j_s(\omega) \tag{6}$$

where S is usually referred to as an order parameter or the residual anisotropy and $j_f(\omega)$ and $j_s(\omega)$ are the spectral densities that densities that describe the fast and slow motions respectively. Here it is also assumed that the fast local motions have a threefold or higher symmetry around an average molecular orientation (normal to the surfactant film). In the case of particles it can further be assumed that the fast motions are in extreme narrowing conditions and hence the difference $\Delta R (\equiv R_2 - R_1)$ depends only on the slow dynamics. For the large particle dimensions of the present system, the dynamics associated with the aggregates are slow compared to the inverse resonance frequency. Hence, we can use the approximation :

$$\Delta R = \frac{9\pi^2}{40}|\chi S|^2 j_s(0)\,. \tag{7}$$

This equation has been applied to a similar study on reverse micelles [28]. Keeping the total area to enclosed volume ratio of the swollen micelles fixed, as done in this study, measurements of ΔR provides a simple and accurate method to monitor a swollen micellar growth [28, 29].

The absolute value of product $|\chi S|$ can be determined in anisotropic liquid crystalline phases from quadrupolar splittings. For the case of a lamellar phase, the quadrupolar splitting, Δ is given by :

$$\Delta = \frac{3}{4}|\chi S|\,. \tag{8}$$

In general, $|\chi S|$ is experimentally found to be independent of the aggregate geometry, and for a given surfactant a similar value is found in the micellar and liquid crystalline phases [25-27]. In the present lamellar phase, however, $|\chi S|$ is further reduced due to bilayer undulations, and to find the $|\chi S|$ value associated with the total anisotropic motions only, we need to evaluate Δ at high surfactant plus oil concentration where the undulations are damped out.

4. Results.

The temperatures of the upper and lower phase boundaries of the microemulsion phase are listed for the different samples of the present study in table I.

The transverse and longitudinal relaxation times were measured as a function of Φ along the emulsification failure boundary. At 25.5 °C, R_1 was observed to be $32 \pm 1\ s^{-1}$ and

Table I. — *Phase boundary temperatures for the microemulsion phase of the samples examined in the relaxation and self-diffusion studies. The phase transition temperatures were determined optically as described in the text.*

Volume fraction Φ	Upper phase boundary (°C)	Lower phase boundary (°C)
0.230	32.4	25.4
0.117	32.6	25.6
0.059	32.5	25.7
0.024	32.5	25.7
0.012	32.6	25.7

independent of the concentration. At the highest temperature studied in the microemulsion phase, 31 °C, R_1 was 28 s^{-1} at the lowest and 28.1 s^{-1} at the highest concentration, with the corresponding R_2 values being 303 s^{-1} and 1 000 s^{-1} The fact that R_1 is experimentally found to be constant while R_2 varies with the concentration signifies that the variation in R_2 results essentially from a variation in $j_s(0)$ and the slow motion does not contribute to R_1. Hence, with $R_2 \gg R_1$ we have $j_s(0) \gg j_s(\omega)$ and we may safely use the approximation $\Delta R \propto j_s(0)$ (Eq. (7)).

Figure 2 shows the variation in the quantity ΔR as a function of Φ for four different temperatures in the microemulsion phase. The lowest temperature, 25 °C, is slightly below the lower phase boundary. However, samples left a few degrees below the lower phase boundary are observed to be metastable on a time scale of hours. In the vicinity of the lower phase

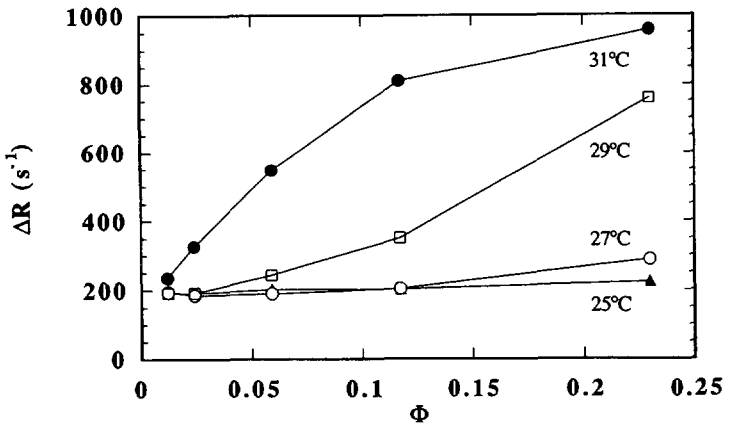

Fig. 2. — The variation of the observed relaxation rate difference, ΔR, as a function of sample concentration at four temperatures in the microemulsion phase. Note that the phase boundaries for the microemulsion phase are not included in this figure, or subsequent temperature dependence figures, but they are placed in table I.

boundary, the relaxation rates are temperature independent, and the measurements performed on the metastable samples represent the micellar properties at the lower phase boundary. At 25 °C, ΔR is virtually concentration independent, while at higher temperatures ΔR increases with Φ. The increase is stronger the higher the temperature. For the more concentrated samples, $\Phi = 0.117$ and 0.230, respectively, figure 3 shows the evolution of ΔR plotted as a function of temperature for the samples upon cooling through the microemulsion phase. An important observation here is that ΔR levels off at lower temperatures.

Complimentary information to the relaxation data can be obtained from molecular self-diffusion measurements. In figure 4 we show the variation with temperature of the self-diffusion coefficients of the surfactant and oil, respectively for the two samples with $\Phi = 0.117$ (Fig. 4a) and $\Phi = 0.230$ (Fig. 4b).

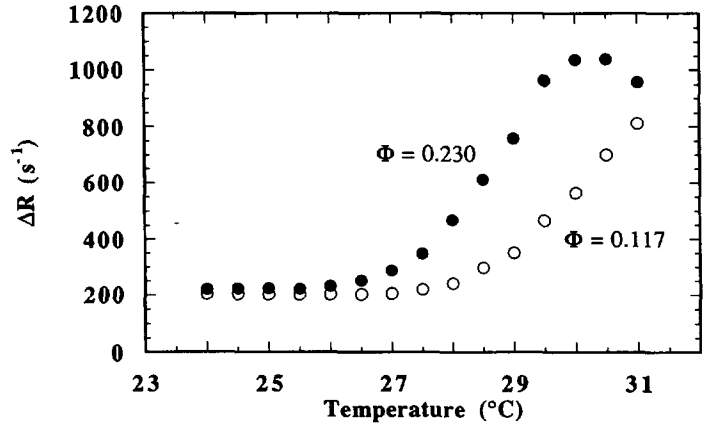

Fig. 3. — Temperature dependence of the observed relaxation rate difference, ΔR, upon cooling through the microemulsion phase for the concentrated samples, with volume fractions (Φ) of 0.117 and 0.230.

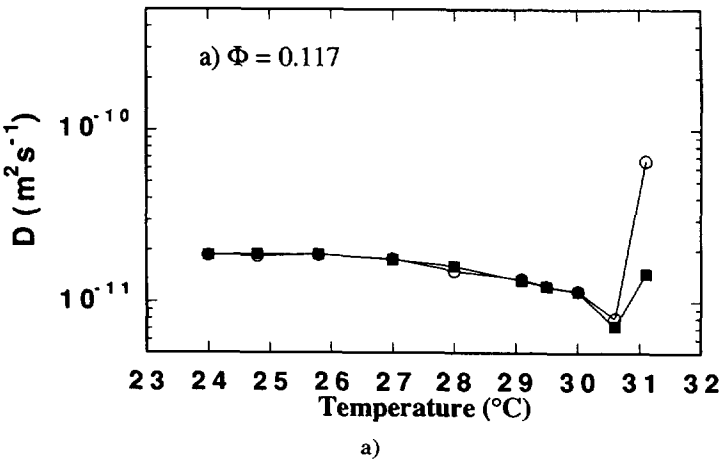

Fig. 4. — Temperature dependence of the (○) oil and (■) surfactant self diffusion coefficients across the microemulsion phase for : (a) the $\Phi = 0.117$ sample and (b) the $\Phi = 0.230$ sample, using the ^1H FTPGSE self diffusion technique.

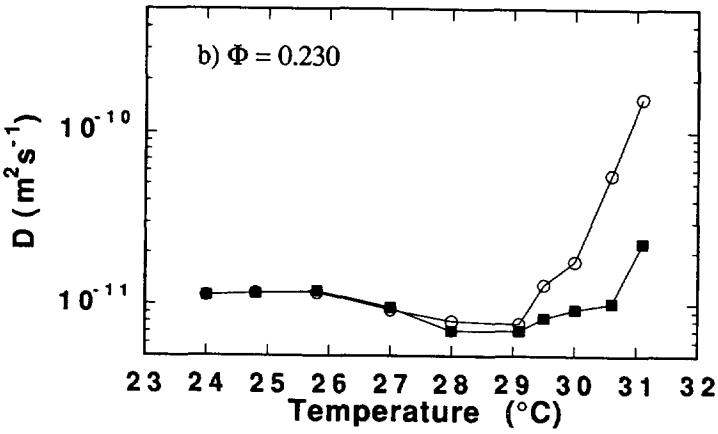

b)

Fig. 4 (*continued*).

Quadrupolar splittings, which were used in the calculation of $|\chi S|$, were measured in the lamellar phase at 37 °C for four different concentrations, and the values shown in table II. The magnitude of the quadrupolar splitting decreases with dilution. A similar decrease has been observed in the binary water-$C_{12}E_4$ lamellar phase [30]. This decrease is attributed to the increased amplitude of the undulations in the lamellae as the periodicity increases. Due to the finite size, the micelles in the microemulsion phase have restricted shape fluctuations. Hence we are only interested in the residual anisotropy after partial averaging of the quadrupolar interaction due to local molecular motions, which we expect to be given by the limiting value of the quadrupolar splitting at higher concentrations, in the lamellar phase. In subsequent calculations we use a value for $|\chi S|$ as obtained from the splitting in the most concentrated sample ($\Phi = 0.594$).

Table II. — *Quadrupolar splittings* (Δ) *measured in the lamellar phase of the studied system at* 37 °C.

Volume fraction Φ	Quadrupolar splitting Δ (Hz)
0.117	7 860
0.230	8 300
0.564	9 970
0.594	10 300

Dynamic light scattering measurements were performed on some dilute samples ($\Phi < 0.06$) at 25.0 °C, close to the lower phase boundary. The obtained collective diffusion coefficients, D_c, are plotted as a function of Φ in figure 5. The solid line is a linear fit to the data yielding $D_c/D_0 = 1 + 0.88\ \Phi$, where the infinite dilution value $D_0 = 2.6 \times 10^{-11}\ m^2\ s^{-1}$ is consistent with a hydrodynamic radius $r_H = 94$ Å.

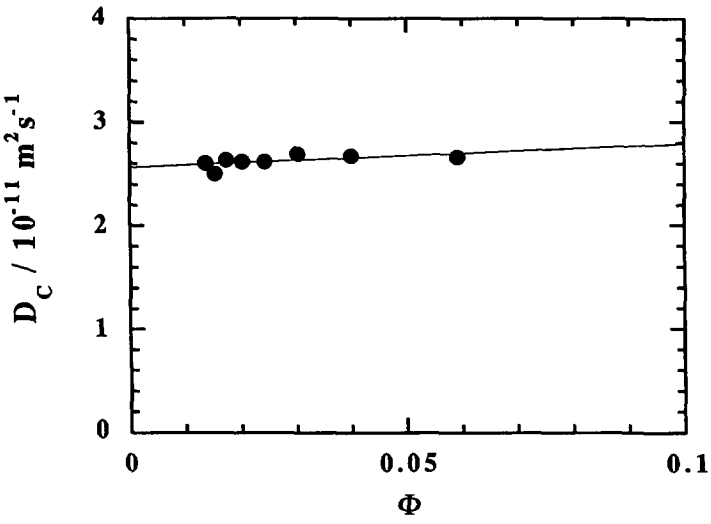

Fig. 5. — The collective diffusion coefficient, D_c, as a function of the volume fraction, Φ, of surfactant and oil, measured at 25.0 °C using dynamic light scattering.

5. Discussion.

The present study concerns a water-rich ternary micro-emulsion. Fixing the surfactant-to-oil ratio corresponds to fixing the total area-to-enclosed volume ratio of normal, oil-swollen micelles. Spherical micelles can be viewed as consisting of a spherical hydrocarbon core, containing the oil and the hydrocarbon tails of the surfactant, covered with a layer of end-anchored pentaethylene oxide chains, as illustrated schematically in figure 6. The volume of

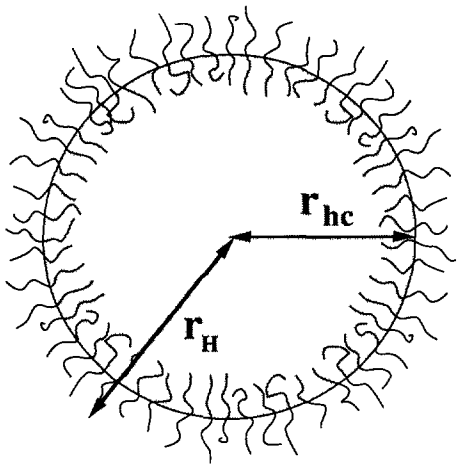

Fig. 6. — A schematic representation of an oil swollen spherical micelle. Here we indicate the different radii described in the text. These radii are denoted by r_H and r_{hc}. In the text these radii are referred to as the hydrodynamic and hydrocarbon radius respectively. The hydrocarbon radius defines the sphere that encloses all the oil and the hydrocarbon chains of the surfactant. It measured to the apolar-polar interface where the head groups join the hydrocarbon chain.

the $C_{12}E_5$ hydrocarbon chain corresponds to approximately half of the total surfactant volume, v_s, and the radius of the hydrocarbon core is given by :

$$r_{hc} = \frac{3(\Phi_0 + (\Phi_s/2))\,\ell_s}{\Phi_s} \tag{9}$$

Here, $\ell_s = v_s/a_s$ is the surfactant length where a_s is the area per surfactant molecule at the polar-apolar interface associated with r_{hc}. A value for the length of the $C_{12}E_5$ surfactant, $\ell_s = 15$ Å, has been found in hexagonal and lamellar phases of the $C_{12}E_5$-water-tetradecane system [12] and in the binary water-$C_{12}E_5$ system [13]. This value is essentially independent of the temperature and the aggregate geometry. Upon substituting this ℓ_s value into equation (9), we obtain $r_{hc} = 78$ Å.

For a given ratio of surface area to enclosed volume the particle of smallest size is a sphere. At the same surface area to enclosed volume larger particles will have a non-spherical shape. The experimental techniques involved in this study are sensitive to the size of the aggregates, but not to the shape. In the analysis of micellar growth we will assume a prolate shape for the micelles. Prolates and oblates are well defined non-spherical shapes, for which there also exist numerical solutions to the joint spectral density function entering the expressions for the NMR relaxation rates. Focusing on a one (prolate) rather than a two-(oblate) dimensional growth corresponds to assuming the shape transitions to follow the sequence sphere-to-cylinder-to-lamellae [31]. Further justification for the choice of one-dimensional micellar growth is obtained from the presence of a hexagonal phase at higher concentrations in the phase diagram (unpublished results).

In the following, the discussion is split into three main sections. Firstly we will consider the implications of the results we have achieved along the lower phase boundary and then go on to interpret the relaxation and self-diffusion results obtained upon increasing the temperature away from this boundary. Finally we compare our experimental findings with the predictions of the flexible surface model.

5.1 MICELLAR SHAPE AND SIZE ON THE LOWER PHASE BOUNDARY. — It is clear from figures 2 and 3 that ΔR levels off at a minimum value at the emulsification failure boundary and that this quantity is constant along this isotherm. This levelling off of ΔR to a minimum value is most clearly demonstrated in figure 3. Measurements were performed also below the lower phase boundary, on metastable samples, to ensure that there was no further decrease in the micelle size (phase separation below this boundary is observed to be very slow). ΔR levels off to its minimum value above the lower phase boundary, indicating that the aggregates have a minimum size at the phase boundary and that the aggregate size there is invariant with respect to the concentration. Noting that for a given interfacial area-to-enclosed volume the smallest particle corresponds to a spherical shape we conclude from these results that the oil-swollen micelles are close to spherical on the lower phase boundary, and that their size does not change along this phase boundary within the investigated concentration range.

Further support for this conclusion can be gained from the NMR self-diffusion studies carried out along this boundary for the $\Phi = 0.117$ and 0.230 samples. Here, whilst we can say very little directly about the micelle shape, the surfactant and oil diffusion coefficients correspond to the micellar self-diffusion constant, D_{mic}, because the surfactant and oil diffuse with the same diffusion coefficient and hence are present in the same aggregate. Below 27 °C for $\Phi = 0.117$ and 26 °C for $\Phi = 0.230$, D_{mic} is constant, within experimental error, indicating a constant micellar size. D_{mic} takes a maximum value consistent with a minimum in the micelle size.

From the measured relaxation rate difference along at the lower phase boundary we can now

proceed and estimate a radius of the micelles, assuming a spherical shape. For spherical particles, $j_s(\omega)$ is Lorentzian and in particular $j_s(0) = 2\ \tau_s$, where τ_s is the correlation time in an exponential time auto correlation function of the slow motion. Due to the internal degrees of freedom, τ_s has contributions from both the aggregate tumbling (τ_t) and the surfactant lateral diffusion within the interfacial film (τ_d). These two processes may be considered to be statistically independent in which case it is possible to write

$$\tau_s^{-1} = \tau_t^{-1} + \tau_d^{-1} \tag{10}$$

For the tumbling, we consider the rotational diffusion of a sphere of radius r_H, where r_H is the hydrodynamic radius. This correlation time is given by :

$$\tau_t = \frac{4\ \pi\ \eta r_H^3}{3\ k_B\ T} \tag{11}$$

where η is the solvent viscosity and $k_B\ T$ the thermal energy.

The lateral diffusion coefficient of the surfactant molecules is naturally defined at the polar-apolar interface, of radius r_{hc}, dividing the ethylene oxide from the hydrocarbon part of the surfactant monolayer as illustrated in figure 6. In this case, the correlation time associated with the lateral diffusion is given by :

$$\tau_d = \frac{r_{hc}^2}{6\ D_{lat}} \tag{12}$$

While τ_d is well defined, D_{lat} is only well defined when the surface on which the diffusion is evaluated is specified. This is particularly important when comparing D_{lat} values from different structures.

The quadrupolar splittings from the lamellar phase show a strong variation with the concentration. Since the present non-ionic lamellar phase swell by means of the undulation force, we expect an additional averaging of the quadrupolar coupling due to the partially crumpled bilayers. The order parameter, S, associated with the local molecular motions hence corresponds to the limiting quadrupolar splitting at high surfactant concentration where the undulations are damped out. Assuming S to be given by the quadrupolar splitting at the highest concentration measured, $\Delta R = 205\ s^{-1}$ as measured on the lower phase boundary (mean value from the four lowest concentrations), corresponds to $\tau_s = 2.4 \times 10^{-7}$ s.

D_{lat} can be measured directly in systems of infinite films such as bicontinuous microemulsions, cubic phases, sponge phases etc. [32]. In the bicontinuous cubic phase, formed in the binary $C_{12}E_5$-water system, D_{lat} was found to be $3 \times 10^{-11}\ m^2\ s^{-1}$ at 20 °C [12]. With this value and a water viscosity of 0.89 cp, we can now proceed and calculate radius *via* equations (10-12). The uncertainties in D_{lat} and $|\chi S|$, which we estimate to 10-20 %, are of the same order as the relative difference in r_H and r_{hc}, hence this resolution does not justify a determination of the latter two quantities. We simplify the analysis and represent the micellar size in terms of a single radius only, making the approximation $r_{hc} \approx r_H \approx r$ in equations (11) and (12). Using the values of the different parameters stated above, we obtain a radius, r, for the spherical micelles of 86 Å. This value (representing an effective mean of r_H and r_{hc}) is consistent with the values, $r_{hc} = 78$ Å and $r_H = 94$ Å, obtained from the ℓ_s value (Eq. (9)) and the DLS experiment, respectively. Alternatively, we can calculate τ_s and ΔR using the above stated values for r_{hc} and r_H. Using the same values for D_{lat}, $|\chi S|$, and η, we calculate $\tau_s = 2.3 \times 10^{-7}$ s and $\Delta R = 194\ s^{-1}$. The good agreement supports the previous conclusion that the micelles along the lower phase boundary are spherical.

Shape fluctuations are strongly restricted since the surfactant film is practically unstrechable [33]. The effects of shape fluctuations can in principal be taken into account in the evaluation of the relaxation data [34], but are most likely negligible. The effects are largest for slow ($\gg \tau_c$) modes [34], corresponding to a static shape polydispersity. Considering a prolate deformation at constant volume, an axial ratio of 1.5 will in this case increase ΔR by approximately 10 % compared to the spherical case (see also Fig. 7 and the discussion below). Large fluctuations, if present, will affect the evaluated radius, but not the conclusion concerning the minimum micellar size at the lower phase boundary.

A more extensive light scattering study along the lower phase boundary has been performed previously [11], although with heavy water (D_2O) as solvent. The r_H value obtained here (94 Å) is identical to the value, 95 Å [11], obtained in D_2O.

5.2 MICELLAR SIZE AND SHAPE AWAY FROM THE LOWER PHASE BOUNDARY. — The main strength of the ^{2}H-NMR relaxation technique as a complement to other techniques in the study of surfactant aggregate structure is the strong variation of ΔR with micellar size. This property was invoked above where we could conclude that the micellar size was minimum, corresponding to a spherical shape, which remained constant along the lower phase boundary. Below we will proceed by analysing the micellar growth as the temperature is increased away from the lower phase boundary.

As the temperature increases the spontaneous radius of curvature for the surfactant monolayer is larger than that for the sphere at the given surfactant-to-oil ratio (see Eq. (9)), and other geometries for the aggregates are energetically favoured. However, the entropy of mixing favours small aggregates so the growth is expected to be significantly suppressed at lower Φ, as seen in the experimentally observed results where ΔR increases very little at 31 °C from its value at 25 °C for the $\Phi = 0.019$ and 0.024 samples.

A quantitative analysis of the effect of micellar growth on ΔR can be performed in terms of well defined non-spherical shapes such as prolates. In a previous paper Skurtveit and Olsson [28] have used Halle's [29] numerical treatment of the joint spectral density function of lateral

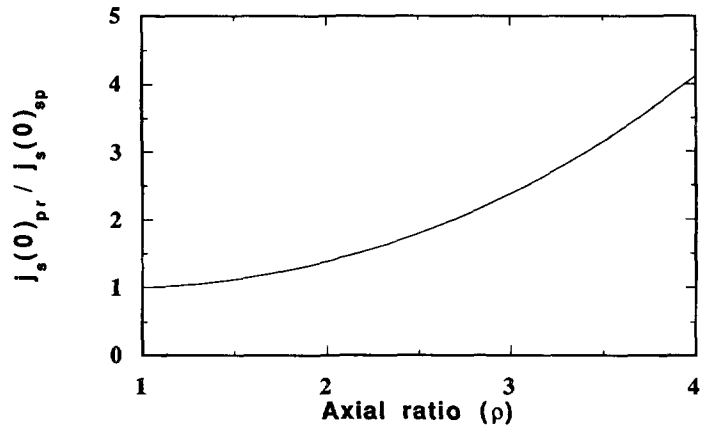

Fig. 7. — Calculated ratio of the zero frequency joint spectral densities of a prolate spheroid to that of a sphere plotted as a function of axial ratio, ρ. The calculations are made using Halle's [29] theory and utilising a constant area to enclosed volume of 0.039 $Å^{-1}$ and a lateral diffusion coefficient of 3×10^{-11} $m^2 s^{-1}$

diffusion and tumbling of prolate spheroids, to quantitatively analyse a particle growth in a microemulsion system. Following the approach of reference [28] we have calculated the ratio, $j_{s,\,pr}(0)/j_{s,\,sph}(0)$, of the zero frequency spectral density functions for a prolate ($j_{s,\,pr}(0)$) and a sphere ($j_{s,\,sph}(0)$), where the prolate and the sphere have the same ratio of surface area to enclosed volume, which we in this study have fixed globally by a constant surfactant-to-oil ratio, see figure 7. Keeping this constraint on a local level also amounts to the describing the particles as being monodisperse. Since we have no detailed information on the size and shape polydispersity, the result of the calculations should be considered as an estimate of the average particle size, expressed in terms of monodisperse prolates.

By using the ratio $j_{s,\,pr}(0)/j_{s,\,sph}(0) = \Delta R_{pr}/\Delta R_{sph}$ we have excluded the uncertainty associated with the value of the order parameter and we focus only on the variation of $\Delta R = \Delta R_{pr}$ relative to a reference, ΔR_{sph}, corresponding to the spherical shape, which we take as the limiting ΔR value at the lower phase boundary. For simplicity we describe the micelles by a single interface, which for the reference spherical state corresponds to a radius of 86 Å, and we have used $D_{lat} = 3 \times 10^{-11}\ m^2\ s^{-1}$ We have also neglected the small variation in the water viscosity with temperature and constantly used the 25 °C value $\eta = 0.89$ cp.

The results of the calculations applied to the temperature variation of ΔR for the $\Phi = 0.117$ and 0.230 samples (Fig. 3) are presented in figure 8 as the prolate axial ratio, ρ, (defined as $\rho \geq 1$) as a function of temperature through the microemulsion phase.

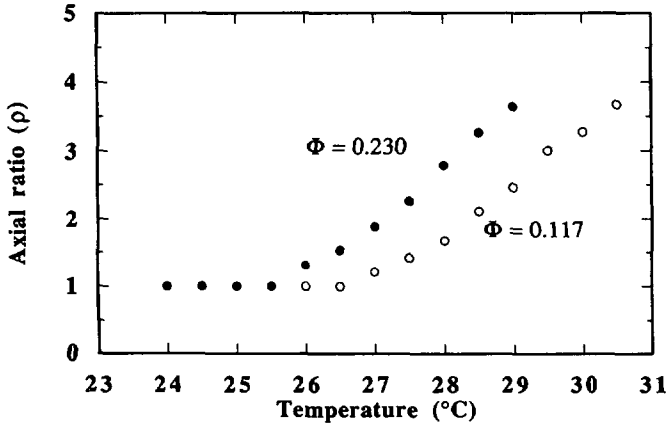

Fig. 8. — Calculated axial ratios for the prolate spheroids as a function of temperature for the two samples studied in the self-diffusion experiments (with (○) denoting the $\Phi = 0.117$ results and (•) denoting the $\Phi = 0.230$ results) in the microemulsion phase. Note that for the $\Phi = 0.230$ sample these calculations are presented for temperatures below the maximum in the ΔR values from the relaxation study were the surfactant and oil diffusion coefficients become different indicating a transition to a bicontinuous microstructure.

For the $\Phi = 0.230$ sample we have only included temperatures below the maximum in ΔR, since above this temperature the microstructure is bicontinuous as demonstrated by the dramatic increase of the oil and surfactant self-diffusion coefficients. Similar ΔR maximum coinciding with a diffusion coefficient minimum has been observed in related systems [35, 36].

The particles grow only moderately with increasing temperature, with the maximum size corresponding to an axial ratio of approximately 3.5. For the $\Phi = 0.117$ sample there is a similar increase in the size of the micelles, although slightly less pronounced. For the lower

concentrations, the ΔR values obtained at 31 °C (Fig. 2) correspond to an axial ratio of about 3.3 and 2.5 for the $\Phi = 0.059$ and 0.024 respectively. For the lowest concentration, $\Phi = 0.012$, ΔR at 31 °C indicates an axial ratio of about 1.8. We also note that for the two lowest concentrations deviations from spherical shape occur first when the temperature exceeds 29 °C.

The self-diffusion data presented in figure 4 for the $\Phi = 0.117$ and 0.230 samples confirm the conclusions based on the relaxation experiments. At lower temperatures the surfactant and oil diffusions coefficients are equal proving that the microstructure is that of discrete oil swollen micelles. Increasing the temperature, D_{mic} decreases indicating a micellar growth. Above 31 °C for $\Phi = 0.117$ (just below the upper phase boundary) and above 29 °C for $\Phi = 0.230$ the self-diffusion coefficients increase dramatically with increasing temperature, indicating a cross over to a bicontinuous microstructure. Here the oil diffusion coefficient is higher than that of the surfactant, mainly due to a higher local mobility of the oil over that of the surfactant (the bulk self-diffusion coefficient of decane is over an order of magnitude higher than the lateral diffusion coefficient of $C_{12}E_5$ within the film). Since this paper is primarily concerned with the discrete particle microstructures we will take the discussion of the transition to the bicontinuous structure no further. Similar relaxation and self diffusion results have been observed in other microemulsion systems [35, 36] and this transition is dealt with in more detail there.

The decrease in D_{mic}, due to micellar growth, with increasing temperature away from the lower phase boundary is partially due to a decrease of the free particle diffusion coefficient [37], $D_0 = k_B T/(6 \pi \eta r_H)$, associated with an increase in r_H, and in addition a concomitant increase in the excluded volume. Although the latter effect is less well-known, it is clear that the self-diffusion data support the conclusion from the relaxation study that the micellar growth is only minor.

5.3 STRUCTURE AND PHASE EQUILIBRIA WITHIN THE FLEXIBLE SURFACE MODEL. — Summarizing the conclusions from the experimental results we have found that : (i) the swollen micelles are spherical on the lower phase boundary over the whole concentration range studied. (ii) At temperatures above the lower phase boundary, the micelles grow in size with increasing concentration. The micelles grow more rapidly with concentration, the higher the temperature. (iii) An important observation is that the micellar growth is nevertheless only minor. The largest average particle size observed is consistent with a prolate micelle with an axial ratio of approximately 3.5.

The phase behaviour of the present system (Fig. 1b), as well as the observation of a particle growth with increasing temperature, are consistent with the assumption that H_0 decreases with increasing temperature. Spherical oil-swollen micelles are indeed predicted to coexist with excess oil and we can identify the lower phase boundary with the emulsification failure boundary, discussed by Safran and co-workers [14].

It is of interest to compare the spontaneous radius of curvature, $r_0 \equiv H_0^{-1}$, with the stoichiometric spherical radius r, dictated by the surfactant-to-oil ratio, which we here identify with r_{hc} (defined in Eq. (9)). Above a certain value of the ratio r/r_0, phase separation with excess oil occurs. Including an ideal entropy of mixing of micelles and solvent molecules, equilibrium with excess internal phase (oil) occur at [15] :

$$\frac{r}{r_0} = 1 + \frac{\bar{\kappa}}{\kappa} + \frac{k_B T}{4 \pi \kappa} \ln \{X\} \, . \tag{13}$$

Here the last term results from the entropy of mixing, where X is the molar fraction of micelles. We see here, that equation (13) predicts that r/r_0 on the emulsification failure boundary increases as the concentration of micelles decreases.

A striking observation is that the phase boundary is a straight line up to high volume fractions, $\Phi \leq 0.35$. This is a general behaviour observed for a number of non-ionic surfactant water oil systems [4, 38], and is consistent with a concentration independent r/r_0 on the phase boundary. This indicates that the variation of last term in equation (13) is negligible in comparison to $1 + \bar{\kappa}/\kappa$. The analysis can be carried further if we consider the explicit temperature dependence of H_0 and the resolution of the phase boundary determination. However, a more detailed analysis should also include non-ideal entropy of mixing, which takes into account the (large) difference in size of the micelles and the solvent (water) molecules. Work is progressing in these areas.

Acknowledgements.

This work was supported by the Swedish Natural Science Research Council (NFR). We are grateful to István Furó for his assistance with the relaxation experiments.

References

[1] Helfrich W., *Z. Naturforsch.* **28c** (1973) 693-703.
[2] Wennerström H., Anderson D. M., Statistical Mechanics and Differential Geometry of Micro-Structured Materials, A. Friedman, J. C. C. Nitsche and H. T. Davis Eds. (Springer Verlag, Berlin, 1991).
[3] Mitchell D. J., Tiddy G. J. T., Waring L., Bostock T., McDonald M. P., *J. Chem. Soc. Faraday Trans. 1* **79** (1983) 975.
[4] Kunieda H., Shinoda K., *J Dispersion Sci. Technol.* **3** (1982) 233.
[5] Kahlweit M., Strey R., *Angew. Chem Int. Ed. Engl.* **24** (1985) 654.
[6] Olsson U., Shinoda K., Lindman B., *J. Phys. Chem.* **90** (1986) 4083-4088.
[7] Olsson U., Nagai K., Wennerström H., *J. Phys. Chem.* **92** (1988) 6675-6679.
[8] Anderson D., Wennerström H., Olsson U., *J. Phys. Chem.* **93** (1989) 4243-4253.
[9] Olsson U., PhD Thesis, Lund (1988).
[10] Wennerström H., Olsson U., *Langmuir* **9** (1993) 365-368.
[11] Olsson U., Schurtenberger P., *Langmuir* **9** (1993) 3389-3394.
[12] Olsson U., Würz U., Strey R., *J. Phys. Chem.* **97** (1993) 4535-4539.
[13] Strey R., Schomäcker R., Roux D., Nallet F., Olsson U., *J. Chem. Soc. Faraday Trans.* **86** (1990) 2253-2261.
[14] Turkevich L. A., Safran S. A., Pincus P. A., Surfactants in Solution, K. L. Mittal and P. Bothorel Eds. (Plenum Press, New York, 1986), Vol. 6, pp. 1177-1191.
[15] Safran S. A., Structure and Dynamics of Strongly Interacting Colloids and Supramolecular Aggregates in Solution, S. Chen, J. S. Huang and P. Tartaglia Eds. (Kluwer Academic Publishers, Dordrecht, the Netherlands, 1992).
[16] Strey R., Winkler J., Magid L., *J. Phys. Chem.* **95** (1991) 7502-7507.
[17] Davis J. M., Jeffrey K. R., Bloom M., Valic M., Higgs T. P., *Chem. Phys Lett.* **42** (1976) 390.
[18] Griffin R. G., *Meth. Enzymol.* **72** (1981) 108.
[19] Stilbs P., *Prog Nucl. Magn. Reson Spectrosc.* **19** (1987) 1-45.
[20] Mills J. R., *J. Phys. Chem.* **77** (1973) 685.
[21] Ertl H., Dullien F. A. L., *AlChE J.* **19** (1973) 1215-1223.
[22] Abragam A., The Principles of Nuclear Magnetism (Clarendon Press, Oxford, 1961).
[23] Wennerström H., Lindman B., Söderman O., Drakenberg T., Rosenholm J. B., *J. Am. Chem. Soc.* **101** (1979) 6860.
[24] Halle B., Wennerström H., *J. Chem Phys.* **75** (1981) 1928.
[25] Lindman B., Söderman O., Wennerstrom H., Surfactant Solutions New Methods of Investigation, R. Zana Ed. (Marcel Dekker, New York, 1987) pp. 295-357.

[26] Söderman O., Walderhaug H., Henriksson U., Stilbs P., *J. Phys. Chem.* **89** (1985) 3693.
[27] Söderman O., Henriksson U., Olsson U., *J. Phys. Chem.* **91** (1987) 116.
[28] Skurtveit R., Olsson U., *J. Phys. Chem* **96** (1992) 8640.
[29] Halle B., *J. Chem. Phys.* **94** (1991) 3150.
[30] Olsson U., Strey R., Unpublished.
[31] Safran S. A., Turkevich L. A., Pincus P. A., *J. Phys. Lett.* **45** (1984) L 69.
[32] Anderson D. M., Wennerström H., *J. Phys. Chem.* **94** (1990) 8683-8694.
[33] Faucon J. F., Mitov M. D., Méléard P., Bivas I., Bothorel P., *J. Phys. France* **50** (1989) 2389-2414.
[34] Kenéz P. H., Carlström G., Furó I., Halle B., *J. Phys. Chem.* **96** (1992) 9524-9531.
[35] Olsson U., Jonströmer M., Nagai K., Söderman O., Wennerström H., Klose G., *Progr. Colloid Polym Sci.* **76** (1988) 75-83.
[36] Olsson U., Ström P., Söderman O., Wennerström H., *J. Phys. Chem.* **93** (1989) 4572.
[37] Hiemenz P. C., Principles of Colloid and Surface Chemistry ; 2nd ed. (Marcel Dekker Inc., New York, 1986).
[38] Kahlweit M., Strey R., Busse G., *J. Phys. Chem.* **94** (1990) 3881-3894.